GA–A25595

PROGRESS TOWARD HIGH PERFORMANCE STEADY-STATE OPERATION IN DIII-D

by
C.M. GREENFIELD, M. MURAKAMI, A.M. GAROFALO, J.R. FERRON, T.C. LUCE, M.R. WADE, E.J. DOYLE, T.A. CASPER, R.J. JAYAKUMAR, C.E. KESSEL, J.E. KINSEY, R.J. LA HAYE, J. LOHR, M.A. MAKOWSKI, M. OKABAYASHI, C.C. PETTY, T.W. PETRIE, R.I. PINSKER, R. PRATER, P.A. POLITZER, H. REIMERDES, J.T. SCOVILLE, H.E. ST. JOHN, E.J. STRAIT, and T.S. TAYLOR

OCTOBER 2006

GENERAL ATOMICS

DISCLAIMER

GA–A25595

PROGRESS TOWARD HIGH PERFORMANCE STEADY-STATE OPERATION IN DIII-D

by
C.M. GREENFIELD, M. MURAKAMI,* A.M. GAROFALO,† J.R. FERRON, T.C. LUCE, M.R. WADE, E.J. DOYLE,‡ T.A. CASPER,¶ R.J. JAYAKUMAR,¶ C.E. KESSEL,§ J.E. KINSEY,# R.J. LA HAYE, J. LOHR, M.A. MAKOWSKI,¶ M. OKABAYASHI,§ C.C. PETTY, T.W. PETRIE, R.I. PINSKER, R. PRATER, P.A. POLITZER, H. REIMERDES,† J.T. SCOVILLE, H.E. ST. JOHN, E.J. STRAIT, and T.S. TAYLOR

This is a preprint of a paper to be presented at the 21st IAEA Fusion Energy Conference, October 16-21, 2006, in Chengdu, China, and to be published in the *Proceedings.*

*Oak Ridge National Laboratory, Oak Ridge, Tennessee.
†Columbia University, New York, New York.
‡University of California-Los Angeles, Los Angeles, California.
¶Lawrence Livermore National Laboratory, Livermore, California.
§Princeton Plasma Physics Laboratory, Princeton, New Jersey.
#Lehigh University, Bethlehem, Pennsylvania.

Work supported by
the U.S. Department of Energy
under DE-FC02-01ER54698, DE-AC05-00OR22725, DE-FG03-89ER53297, DE-FG03-01ER54615, W-7405-ENG-48, DE-AC02-76CH03073, and DE-FG02-92ER54141

GENERAL ATOMICS PROJECT 30200
OCTOBER 2006

GENERAL ATOMICS

Abstract

Advanced Tokamak research in DIII-D aims to establish a scientific basis for steady-state high performance scenarios. Recently, $\beta_N \approx 4 \approx 6\,\ell_i$ has been maintained for 2 s with internal transport barriers, well above the no-wall stability limit. The current profile is broadened by a combination of electron cyclotron current drive (ECCD) and a toroidal magnetic field ramp for improved coupling with the wall and active control coils. In other experiments, fully noninductive conditions, $f_{\rm NI} \approx 100\%$, have been sustained for several confinement times, or about half a current relaxation time (τ_R), with $\beta_N \lesssim 3.5$. $f_{\rm NI}$ increases with both q_{95} and β_N. Since fusion gain decreases with q_{95}, we emphasize increasing β at moderate q_{95}. A new lower divertor cryopump allows access to increased β limits through plasma shaping while maintaining the essential density control for ECCD. Initial results confirm the anticipated access to $\beta_N \approx 4$ in a double-null divertor configuration. Theory-based simulations including new DIII-D capabilities predict in-principle steady-state conditions with high β maintained for several τ_R. Extrapolated to ITER, these results project to steady-state operation with $Q \geq 5$.

1. Introduction

Steady-state operation with $Q \geq 5$ is a high level goal for ITER [1]. This recognizes the benefits of steady-state both for elimination of cyclic fatigue and increased duty cycle in future power plants. Advanced Tokamak (AT) research [2-6] on DIII-D and elsewhere [7-8] aims to establish a scientific basis for scenarios that meet this objective.

For steady-state operation, all of the plasma current must be driven noninductively (without a transformer). Our approach is to maximize fusion power and bootstrap current ($f_{\rm BS}$ = 50%-75%) by operating at high normalized beta $\beta_N \geq 3.5$ and safety factor $q_{\rm min} > 1.5$, and provide the remaining current with neutral beam (NBCD), electron cyclotron (ECCD) and fast wave (FWCD) current drive. Recent efforts focus on two scenarios: One exhibits very high fusion performance, $G = \beta_N H_{89} / q_{95}^2 \leq 0.7$, but is not stationary. Another reaches fully noninductive conditions ($f_{\rm NI} \approx 100\%$) at $G \approx 0.3$, demonstrating the ITER $Q = 5$ steady-state scenario.

The first scenario [2], starts with an elevated q profile ($q_{\rm min} > 2$) and has an internal transport barrier (ITB), two features often incompatible with high β. Access is facilitated by a broad current profile, which couples well to the vessel and control coils that actively control both error fields and the resistive wall mode (RWM). This allows operation above the no-wall

limit to the $n=1$ kink mode, usually near $\beta_N \approx 4\ell_i$. This scenario has demonstrated $\beta_N \approx 6\ell_i \approx 4$ sustained for 2 s. Stability calculations indicate the limit may be much higher. This appears promising for steady-state operation, but this has so far not been demonstrated due to an operational requirement for a toroidal field ramp, which drives some off-axis current.

Efforts in a second scenario [3-6] emphasize optimization of fully noninductive operation. These plasmas have $1.5 < q_{\min} < 2.0$ with weakly reversed shear, $q_0 - q_{\min} \le 0.5$, and can be maintained for several τ_E with $\beta_N \le 3.5$ and all current driven by bootstrap, NBCD and ECCD. Similar plasmas can be maintained with stationary profiles and 5%-10% of the current driven inductively, limited only by the 2 s (about one current redistribution time τ_R [9]), duration of ECCD hardware. This scenario requires low density (for ECCD) and high β_N (for fusion gain and bootstrap current). High q_{95} is beneficial for high noninductive current, but detrimental to fusion performance. Our optimization focuses on increasing the β limit at moderate q_{95} (4.0-5.5). Experiments have demonstrated the essential characteristics of the ITER $Q = 5$ steady-state scenario.

Two recent modifications support our AT research program [5]. A lower divertor cryopump now allows density-controlled operation in both single- and double-null (DND) configurations. Initial experiments are consistent with expectations in that operation in a high triangularity DND allows access to higher β, thereby increasing f_{BS}, external current drive efficiency, and G. New long-pulse gyrotrons, now being commissioned, will increase the ECCD power and extend its 2 s pulse length. This additional off-axis current drive is expected to facilitate both higher β limits and improved capability for active current profile control.

This research is supported by a major integrated modeling effort. Theory-based models are used to design experiments and interpret their results. These are in turn used to further refine the models, resulting in increasing predictive accuracy. Simulations with the new device capabilities predict high performance AT operation for several τ_R. The same models, applied to day-1 capabilities of ITER, indicate good prospects for steady-state scenarios with $Q = 5$.

In Section 2, the first scenario, with nonstationary high fusion performance is introduced. Steady-state optimization is discussed in Section 3. Future applications in DIII-D and ITER are discussed in Section 4. A summary is given in Section 5.

2. High β with Internal Transport Barriers

In recent experiments $\beta_N \approx 4$ has been sustained for up to 2 s with $q_{\min} > 2$, under nonstationary conditions [2]. These discharges have low internal inductance ℓ_i, and $\beta_N > 6\,\ell_i$, well above the no-wall stability limit. They also have high confinement $H_{89} > 2.5$. The fusion gain factor G increases during the discharge (β_N and H_{89} are nearly constant, but q_{95} decreases with the B_T), eventually exceeding 0.7, well in excess of the ITER steady-state scenario. The evolution of such a discharge is shown in Fig. 1. Early neutral beam heating is applied to establish high $q_{\min}$. Off-axis ECCD helps to maintain this state with broad current and pressure profiles. β_N is maintained at approximately 4 using neutral beam feedback. As will be discussed, B_T is ramped to help provide a broad current profile.

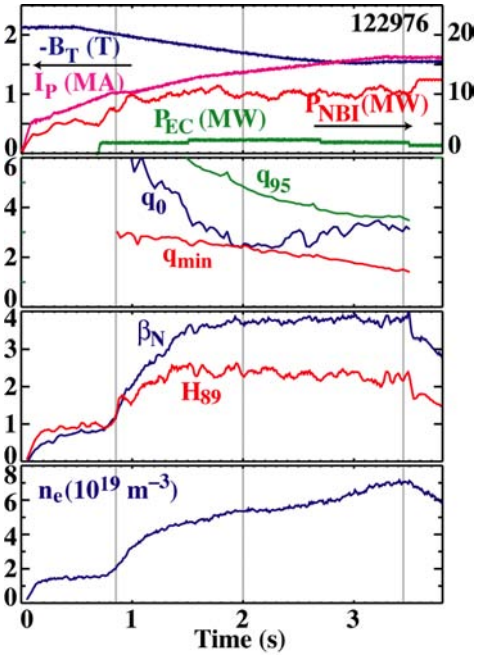

FIG. 1. Time histories of a high β ITB discharge with $\beta_N \approx 4 \approx 6\,\ell_i$. Although β_N is held fixed, I_P, B_T, and density are evolving throughout the discharge.

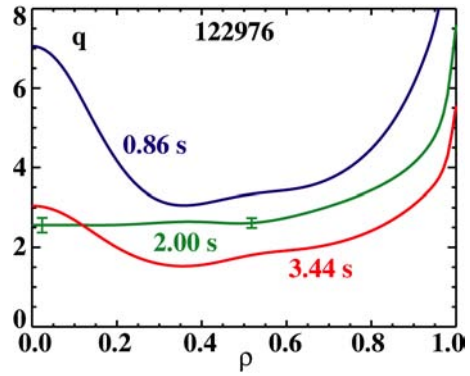

FIG 2. The q profile evolves slowly throughout the duration of the discharge, with $q_{\min} > 2$ maintained for much of the high β_N phase. Profiles shown at times of grey bars in Fig. 1.

The internal magnetic configuration is also dynamic. The q-profile is strongly reversed at the beginning of the high β phase. It becomes flat and then reverses again later in the discharge (Fig. 2), all without significant change to confinement. As $q_{\min}$ evolves, benign tearing modes appear and disappear as it passes through rational values. High performance is usually terminated without disruption by an $(m,n) = (2,1)$ neoclassical tearing mode (NTM) as $q_{\min}$ approaches 1.5. Under fully noninductive conditions, this NTM should be avoided simply by freezing the q-profile.

An ion thermal ITB is a universal feature of these discharges (Fig. 3). It can be seen in both the measured T_i profile and the ion diffusivity determined by analysis with TRANSP [10]. Similar to many other "hot ion" regimes in DIII-D [11], no barrier appears in the other transport channels.

The accessibility of high β under these conditions is unusual in light of earlier observations. Lower stability limits ($\beta_N \leq 3$) usually occur in discharges with ITBs [12] due to the associated highly peaked pressure profile. Also, in the steady-state scenario described in Section 3, high β has usually been difficult to obtain with high $q_{\min}$ [13].

In Fig. 4, the ideal-wall β limit for the $n=1$ kink mode is shown as calculated by DCON [14], indicating that this discharge is stable to $\beta_N \approx 11\,\ell_i > 5$. Further analysis at the time indicated on the figure (2.15 s) finds that the ideal-wall limits to the $n=1$, 2 and 3 kink modes increase with $q_{\min}$ above 2. The no-wall limit does not increase at higher $q_{\min}$, consistent with previous observations [13]. This is partially due to the unusually broad current profile observed in these discharges, which facilitates good coupling with the conducting vessel wall and active stability control coils. A calculated insensitivity to pressure profile peaking may explain the compatibility of the ITB. In these conditions, considerable increases in β may still be possible. These results were made possible by simultaneous feedback control using both internal and external sets of $n=1$ magnetic coils to dynamically correct magnetic error fields and to exert active control of the RWM [15].

This scenario's potential for steady-state is being evaluated. Although many such discharges approach $f_{\mathrm{NI}} \approx 100\%$, $j_{\mathrm{inductive}}$ locally remains finite (Fig. 5). Also, analysis of the current profile [16] indicates substantial current is driven at large radius by the B_T ramp. Although this does not extrapolate to steady-state, it demonstrates the value of far off-axis current drive, which may in future experiments be provided by other means.

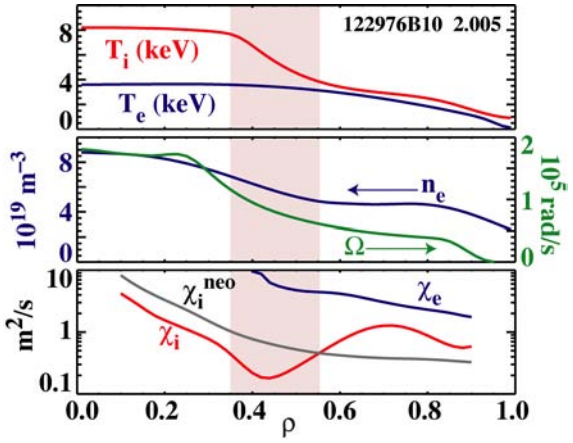

FIG. 3. Profiles during the high β phase indicate the existence of an internal transport barrier in the ion thermal channel. No barrier is evident in the electron channel.

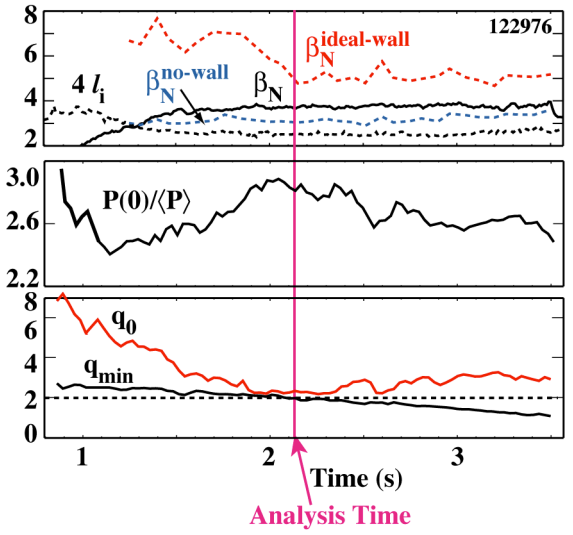

FIG. 4. The calculated ideal-wall β limit for the n=1 kink mode can be up to $11\,\ell_i$, far in excess of the no-wall limit. All available heating power was used in this discharge, limiting attempts to further increase β.

3. Optimization of Steady-State Scenarios

Discharges with $q_{\min}$ = 1.5-2.0, q_{95} = 4-5.5 and weak negative central shear ($q_0 - q_{\min} \leq$ 0.5) form the basis of ITER reference scenario 4 [1], anticipated to demonstrate steady-state with ITER's day-1 configuration. In DIII-D, the desired target q profile is prepared by triggering an L-H transition early in the current ramp (Fig. 6), which slows the current penetration resulting in a broad current profile. During the next 2-3 s, β is slowly increased under feedback control, resulting in a highly reproducible target q profile with $q_{\min} \approx 2$. At this time, the neutral beam power is increased to raise β_N and maintain it at a programmed value, usually about 3.5, and off-axis ECCD is applied.

During this phase, both the total and local inductive current approaches zero (Fig. 7). There are several different ways of determining this. The most straightforward is to calculate the total current profile j_{tot} using an equilibrium reconstruction [18] and the non-inductive current sources using theory-based models. Here we have used Sauter's model for j_{BS} [19], the TRANSP Monte Carlo beam slowing down model [10] for j_{NB}, and TORAY-GA [20] for j_{EC}. The inductive current can be inferred by subtracting the calculated noninductive currents from the total. There is, however, considerable uncertainty in this approach [4]. The equilibrium reconstruction has limited spatial resolution. The bootstrap calculation is sensitive to uncertainties in the profile measurements. The NBCD calculation does not account for redistribution of beam ions by instabilities such as reversed shear Alfvén eigenmodes [21], which can be prevalent in these discharges. A second, more direct, method is to calculate the inductive current directly from the time derivative of the poloidal flux using a series of equilibrium reconstructions [16] ($j_{\text{inductive}}$ in Fig. 7). Comparison between this method and simulations have been successful in reconciling many of the discrepancies [4].

When $f_{NI} \approx 100\%$, the plasma current is supplied by bootstrap (typically 50%-65%), NBCD (20%-35%), and ECCD (5%-10%) [4]. The relatively small current driven by ECCD is nevertheless very important, since both calculation and previous experience [17] show that without it, inductively driven current would replace it near the mid-radius.

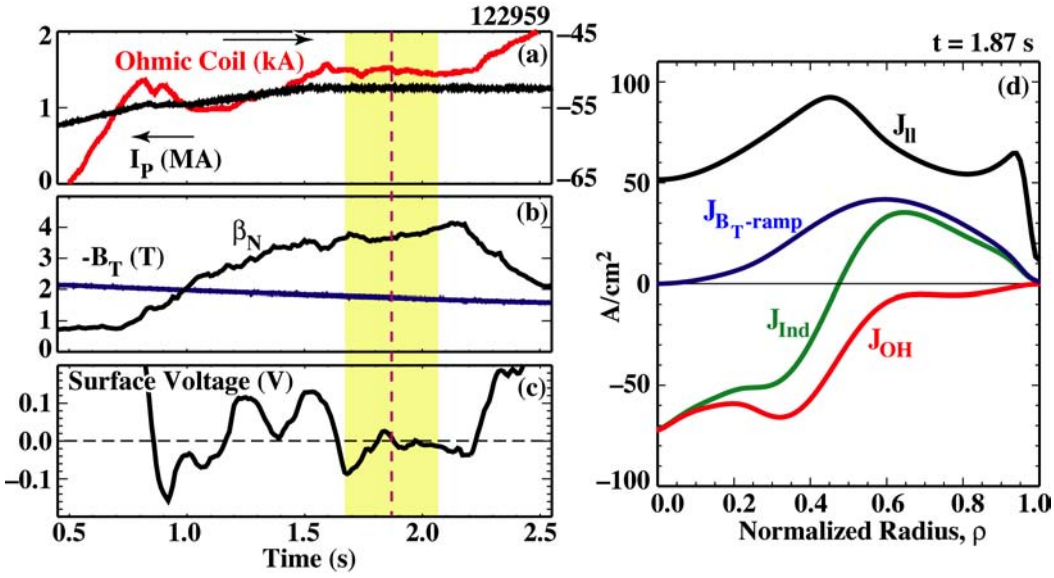

FIG. 5. (a) Plasma (black) and Ohmic transformer (red) currents; (b) β_N and $-B_T$, indicating the ramp; (c) The surface voltage approaches zero, indicating globally $f_{NI} \approx 100\%$; (d) Current profile analysis when $f_{NI} \approx 100\%$ indicating far off-axis current driven by the ramp.

Discharges where the q-profile continues to evolve are usually limited by the onset of an $(m,n) = (2,1)$ NTM. During the fully noninductive phase, this does not occur. These discharges are susceptible to other instabilities as β_N is increased past the no-wall limit [13]. In some cases, these can be a consequence of uncontrolled pressure profile evolution. In other cases, the RWM can limit performance. Active control of the RWM [15] has become an important part of this research since we anticipate routinely operating above the no-wall limit.

We have assembled a global database of about 160 AT discharges with $f_{NI} \geq 80\%$ and durations up to $1 \times \tau_R$ (1-2 s). Figure 8 shows the average noninductive current fraction as a function of β_N for sets of discharges with $q_{95} = 5.0$ and 5.5. These studies clearly indicate the advantages of both high q_{95} and high β_N for AT operation. However, operating with higher q_{95} substantially compromises the fusion performance. We therefore concentrate our optimization on increasing the achievable β_N.

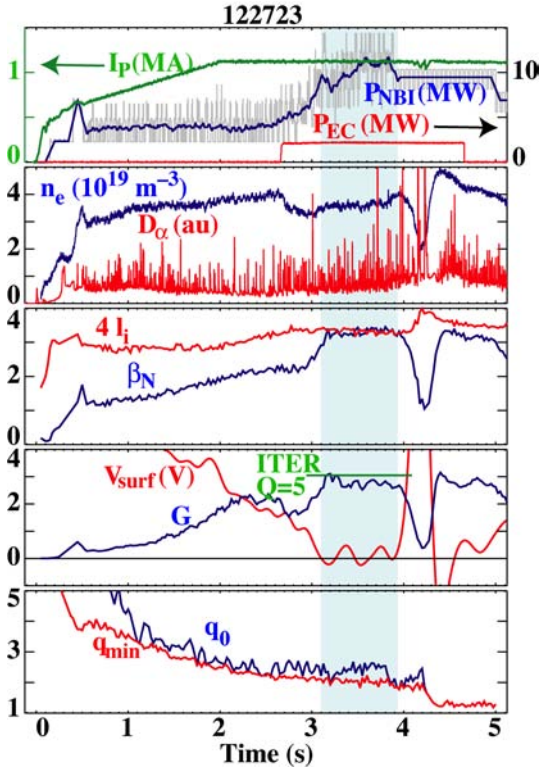

FIG. 6. Time histories of an AT discharge in DIII–D. The shaded region represents the fully noninductive phase.

Previous studies [13] showed that strong shaping can substantially increase the β limit. However, AT plasma shapes are constrained by the need for compatibility with the divertor cryopump geometry for the density control required for effective ECCD [5]. We recently added a high triangularity lower divertor cryopump to allow density control in high

triangularity DND configurations (Fig. 9). Previously, the plasma was formed in an upper single-null (USN) geometry matched to the upper divertor. Recently, we have begun experiments to quantify the benefit of DND operation, where the plasma is vertically symmetrized in a shape otherwise similar to the previous USN (the plasma is magnetically symmetrized and is not optimized to balance the upper and lower particle flows). In first experiments with this configuration, density was controlled, although at higher values than in the upper single-null. These experiments did not attempt to obtain $f_{\mathrm{NI}} \approx 100\%$, partially due to temporarily lower available ECCD power.

An experiment was recently carried out to optimize the DND shape for highest β. Since elongation and triangularity are constrained by the divertor geometry, we chose to test the squareness ζ dependence [Fig. 9(b)]. This is supported by recent calculations indicating significant impact on high β stability (the optimal squareness cannot be predicted quantitatively due to high sensitivity to details of the equilibrium).

The highest values of β_N were achieved at $\zeta \approx 0.33$, equal to that of the previous USN discharges (Fig. 10). Confinement was highest in the same region, with $H_{89} \approx 2.6\text{-}2.9$.

As anticipated, most DND discharges achieved significantly higher β_N, (3.6-4.0) than in the USN shape. Preliminary analysis indicates these plasmas were over a lower range of q_{min} than the USN discharges, but the ranges of q_{min} overlap. The DND discharges achieve superior performance both in terms of fusion gain and expected bootstrap fraction (Fig. 11). Detailed analysis, to determine f_{BS} and f_{NI}, is in progress.

4. Application to Future Experiments in DIII-D and ITER

The most important product of this research is anticipated to be a predictive capability for use in designing AT scenarios for DIII-D and

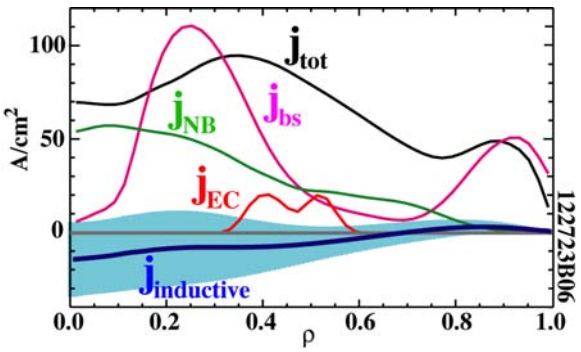

FIG. 7. Components of the current profile during the $f_{\mathrm{NI}} \approx 100\%$ phase.

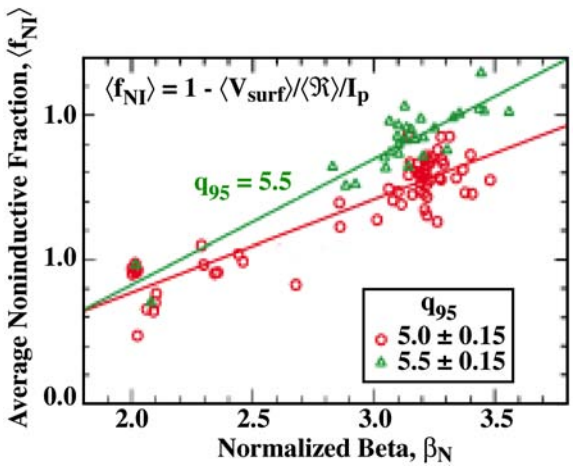

FIG. 8. $\langle f_{\mathrm{NI}} \rangle$ is maximized at both high q_{95} and high β_N in H-mode discharges with weakly negative central shear and $\beta_N > 2$ and $H_{89} > 2$ maintained for at least 0.7 s.

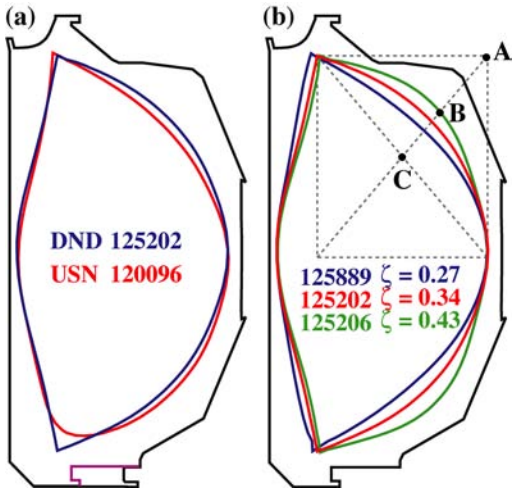

FIG. 9. (a) USN (blue) and DND (red) geometries. Modification for density control shown in magenta. (b) Three discharges from a squareness ($\zeta \equiv BC/AC$) scan.

future devices such as ITER. Our approach couples experimental and integrated modeling efforts; theory-based modeling is used both to design experiments and to interpret their results. For example, the results shown in Section 3 were a direct result of this approach applied to previous experiments [4]. The results also influence the model development, resulting in coupled evolution of the experimental and modeling efforts.

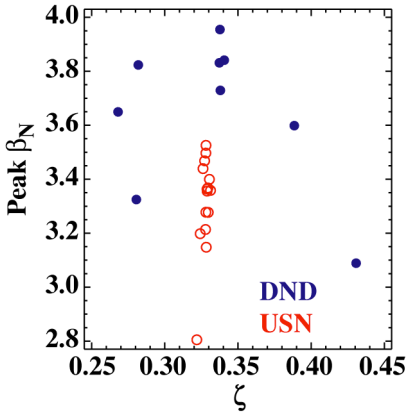

FIG. 10. Double-null discharges obtained increased β_N values compared to the previous USN database, with the highest β_N, approaching 4, achieved at the same squareness as the USN experiments.

Future AT development will be facilitated by hardware improvements now underway in DIII-D [5]. As previously discussed, the highest performance is obtained in a strongly shaped DND. We anticipate further operation with density controlled DND configurations to allow access to $\beta_N \gtrsim 4$. The experiments described here were done with limited ECCD power. The ECCD system is currently being upgraded to six 1 MW, 10 s, gyrotrons. This should be capable of delivering 4.5 MW of power to the plasma, maintained for up to 10 s. Upgrades to the fast wave heating (FWEH) and current drive systems are also near completion.

Figure 12 shows results of a simulation of the current profile components in a $f_{NI} = 100\%$ discharge using these new capabilities [5]. Theory based models calculate the sources and core transport [3] with an empirical pedestal. This approach reproduces most features of the present discharges, and indicates fully noninductive operation at high G in the future. The same approach, applied to ITER with "day 1" capabilities, predicts steady-state performance with $Q = 5$ [1].

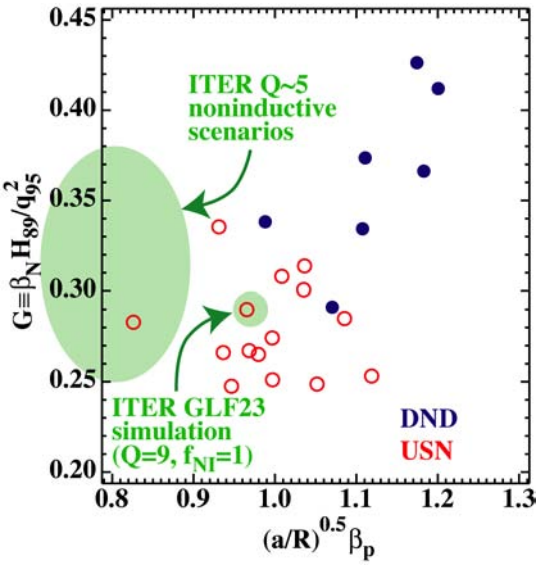

FIG. 11. The recent double-null AT discharges represent improved performance both in terms of fusion gain G *and bootstrap fraction parameter ($(a/R)^{0.5}\beta_P$).*

5. Summary

Recent experiments on DIII-D address the characteristics of two AT scenarios. In the first, $\beta_N \approx 6\,\ell_i \approx 4$ and $G \leq 0.7$ are achieved. These discharges exhibit many desirable AT features, but a continual ramp of the toroidal magnetic field is required. This appears to directly broaden the current profile, thereby aiding in high β stability, even with the appearance of an ITB. In this scenario, the ideal wall limit to the $n = 1$ kink mode is predicted at $\beta_N \approx 11\,\ell_i$. Operating above the no-wall limit requires active magnetic error field correction and RWM stabilization, which are enabled by internal and external control coils. Although not stationary, this scenario confirms the benefits of driving noninductive current far from the axis.

We have also continued developing steady-state high performance in a scenario much like ITER scenario 4. Recent work has focused on identifying parameters for optimization,

especially β_N. A recently added high triangularity divertor cryopump at the bottom of the DIII-D vessel allows access to $\beta_N \le 4$ and $G \le 0.45$ through improved shaping. This, along with additional ECCD and FWCD improvements currently in progress, is expected to enable future DIII-D experiments to demonstrate in principle steady-state AT performance for several τ_R.

Integrated modeling is a crucial tool in the DIII-D AT research program. The same theory-based models that were verified on DIII-D were used to extrapolate from DIII-D to ITER, predicting successful achievement of the ITER $Q = 5$ steady-state scenario.

This work was supported by the U.S. Depart-zment of Energy under DE-FC02-04ER54698, DE-AC05-00OR22725, DE-FG02-89ER53297, DE-FG03-01ER54615, W-7405-ENG-48, DE-AC02-76CH03073, DE-FG02-92ER54141. The authors would like to thank the DIII-D Operations Group for help in carrying out the described experiments.

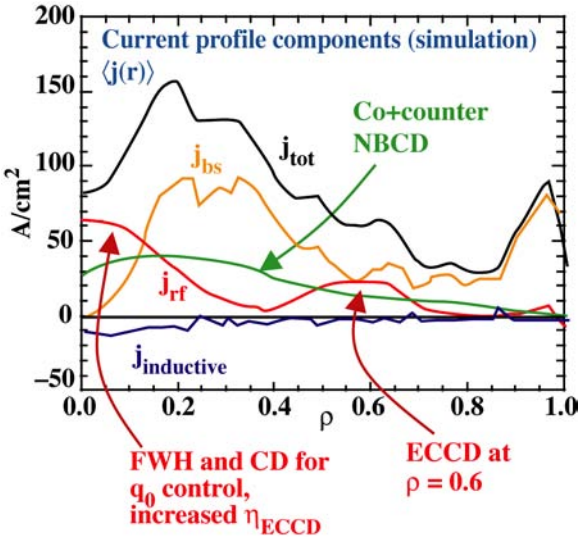

FIG. 12. Theory-based integrated modeling predicts improved performance in future DIII-D AT experiments utilizing recently completed and in-progress hardware upgrades. $P_{EC} = 4.5$ MW, $P_{NB} = 6.8$ MW, $P_{FW} = 3.5$ MW, $I_P = 1.19$ MA, $B_T = 1.86$ T, $\beta_T = 4.1\%$, $\beta_N = 3.8$.

References

[1] HOULBERG, W.A., *et al.*, Nucl. Fusion **45** (2005) 1309-1320.
[2] GAROFALO, A.M., *et al.*, Phys. Plasmas **13**, 056110 (2006).
[3] MURAKAMI, M., *et al.*, Nucl. Fusion **45**, 1419 (2005).
[4] MURAKAMI, M., *et al.*, Phys. Plasmas **13**, 056106 (2006).
[5] GREENFIELD, C.M., *et al.*, Plasma Phys. Control. Fusion **46** (2004) B213.
[6] FERRON, J.R., *et al.*, this conference.
[7] LITAUDON, X., *et al.*, Nucl. Fusion **43** (2003) 565-572.
[8] ISHIDA, S., JT-60 Team and JFT-2M Group, Phys. Plasmas **11** (2004) 2532-2542.
[9] MIKKELSEN, D.R., Phys. Fluids B **1** (1989) 333.
[10] HAWRYLUK, R.J., *An Empirical Approach to Tokamak Transport*, in Physics Close to Thermonuclear Conditions, Edited by B. Coppi *et al.* (Commission of the European Communities, Brussels, 1980) Vol. 1, pp. 19-46.
[11] GREENFIELD, C.M., *et a*l., Phys. Plasmas **4** (1997) 1596-1604.
[12] DOYLE, E.J., *et a*l., Nucl. Fusion **42** (2002) 333-339.
[13] FERRON, J.R., *et al.*, Phys. Plasmas **12** (2004) 056126-1-056126-10.
[14] GLASSER, A.H., and CHANCE, M.S, Bull. Am. Phys. Soc. **42** (1997) 1848.
[15] GAROFALO, A.M., *et a*l., Nucl. Fusion **42** (2002) 1335-1339.
[16] FOREST, C.B., *et a*l., Phys. Rev. Lett. **73** (1994) 2444-2447.
[17] WADE, M.R., *et al.*, Phys. Plasmas **8** (2001) 2208-2216.
[18] LAO, L.L., *et a*l., Nucl. Fusion **30** (1990) 1035-1049.
[19] SAUTER, O., ANGIONI, C., and LIN-LIU, Y.R., Plasmas **6** (1999) 2834-2839.
[20] LIN-LIU, Y.R., CHAN, V.S., and PRATER, R., Phys. Plasmas **10** (2003) 4064-4071.
[21] VAN ZEELAND, M.A., *et al.*. Nucl. Fusion **46** (2006) S880.p